HUNTINGTON MEDICAL RESEARCH INSTITUTES
NEUROLOGICAL RESEARCH LABORATORY
734 Fairmount Avenue
Pasadena, California 91105

Contract No. N01-NS-8-2399

Quarterly Progress Report
July 1-Sept 30, 1999
Report No. 4

"Microstimulation of the Lumbosacral Spinal Cord"

Douglas B. McCreery, Ph. D.
Albert S. Lossinsky, Ph.D.
Leo Bullara, B.A.
Ted G. F. Yuen, Ph.D..
William F. Agnew, Ph.D.

SUMMARY AND ABSTRACT

To date, we have implanted 3 of our new form-fitting, bilateral microelectrode arrays into the sacral spinal cords of 3 cats. In this array, 6 iridium microelectrodes extend, in two rostral-caudal rows of 3, from a single 3 mm epoxy button matrix. The bottom of the button is concave, with a radius of curvature of 2 mm, to conform to the dorsal surface of the S_2 sacral cord. The array is further stabilized by a pair of uninsulated iridium stabilizing pins, 3 mm in length, which extend nearly completely through the sacral spinal cord. The arrays were implanted at a velocity of approximately 2m/sec, using a custom inserter tool, as described previously.

We present histologic findings from the first two animals. Twenty-eight days after implanting the arrays, the cats were anesthetized with Propofol and 2 or 3 of the 6 microelectrodes were pulsed for 12 hours, on each of two successive days. The stimulus waveform was cathodic-first, controlled-current pulses, 150 μs/phase in duration, at a rate of 50 Hz. The stimulus amplitude was 50 or 75μA. The cats were sacrificed immediately after the second 12-hour session. The histologic evaluation testified to the merits of the bilateral form-fitting electrode array. Firstly, the histologic profiles made by the electrodes and stabilization pins indicate that the spinal cord did not rotate during insertion of the electrodes. The saddle-shaped undersurface of the array matrix also appears to be stable on the cord's dorsal surface. There was less injury to the tissue surrounding the electrode tracks than in previous animals in which electrode arrays of other designs had been implanted. However, some gliotic scaring still occurred close to the electrode tracks (usually on only one side of the tracks). This injury was quite minimal in cat sp104, but slightly more severe in cat sp105, in which the array was implanted more caudally in the sacral cord. However, in both animals, there were healthy neurons within 50 μm of the electrode tips. Neurons and neuropil adjacent to the pulsed and unpulsed electrodes appeared essentially identical, and no histological changes attributable to the electrical stimulation were noted. All but three of the neurons near the electrode tip sites appeared to be normal, and the number of neurons within 200 μm of the pulsed and unpulsed electrodes was not significantly different. The tip of one of the 5 pulsed electrodes was surrounded by an aggregate of lymphocytes.

The long stabilizing pins inflicted more tissue injury than did the shorter active electrodes. In the next two animals, we will determine if the long stabilizing pins can be eliminated without compromising the array's mechanical stability.

METHODS

We have implanted 3 of the redesigned electrode arrays into the sacral spinal cords of 3 cats. In this array, 6 iridium microelectrodes extend from a single matrix button 3 mm in diameter. The bottom of the matrix is concave, with a radius of curvature of 2 mm, to conform to the dorsal surface of the sacral cord. The array is further stabilized by a pair of uninsulated iridium anchoring pins, 3 mm in length, which extend nearly completely through the sacral spinal cord. The 6 active electrodes are arranged in 2 rostro-caudal rows, 1.7 mm apart. This is intended to place their tips within the intermediolateral cell column of the S_2 sacral spinal cord when the array's concave bottom is centered over the cord's midline.

The arrays were implanted using aseptic surgical techniques, with the cats anesthetized with Halothane and nitrous oxide. The scalp was opened longitudinally in a midline incision and a percutaneous connector was affixed to the skull. The electrode array was tunneled subcutaneously to the sacral region, and the spinal cord was exposed from L_5 to S_3 with a standard dorsal laminectomy. The L_5 dorsal spinal process was secured with a vertebral clamp and the spinal dura was opened in a longitudinal midline incision extending from S_1 to S_3. The S_2 level of the cord was located approximately by recording the dorsal cord potential while electrically stimulating the perigenital region, which is innervated from the S_2 level of the cord. The arachnoid was then dissected from the spinal roots in the S_2 region, so the roots could be retracted. The recording electrode was inserted through a separate small opening in the dura and passed approximately 4 cm caudally, so as to lie adjacent to the ventral roots. It was then secured to the dura with one additional suture. The recording reference electrode was secured to the outside of the dura at approximately the same level as the recording electrode.

The microelectrode array was then placed into the end of the stator tube (barrel) of inserter tool, where it is held against the armature by a vacuum. The orifice of the barrel was centered over the midline of the sacral cord, with the array cable extending rostrally. The array cable was secured loosely to the dura, approximately 2 cm rostral to the site. The end of the barrel was then used to hold aside the dorsal roots and depress the cord

by approximately 1 mm prior to deploying the array, which was injected into the cord at a velocity of approximately 2 m/sec. After inserting the array, a single 7-0 suture was passed through both margins of the dura and over the array cable, to hold it between the dorsal roots and close to the spinal cord. The dura was then closed loosely, with a pair of 7-0 sutures, and the lips of the cut dura were placed over the array matrix. The partially open dura was covered with a patch of fascia resected from the perispinal muscles. The platinum ground electrode was placed on top of the fascia patch. The perispinal muscles were then approximated with sutures and the skin was closed with staples.

Two of the cats have received stimulation regimens, and have been sacrificed. Twenty-eight days after implanting the arrays, the cats were anesthetized with Propofol and 2 or 3 of the 6 microelectrodes were pulsed for 12 hours on each of two successive days. The stimulus waveform was cathodic-first, controlled-current pulses, 150 μs/phase in duration, at a rate of 50 Hz. The stimulus amplitude was 50 or 75μA. In cat sp104, electrode #1 was pulsed at 50 μA, # 2 was pulsed at 75 μA, and electrodes 3,4,5, and 6 were not pulsed. In cat sp105, electrode #1 was pulsed at 50 μA, and electrodes #2 and #4 were pulsed at 75 μA. Electrodes 3,5 and 6 were not pulsed.

Immediately after the end of the second day of stimulation, the animals were deeply anesthetized with pentobarbital and perfused through the ascending aorta with 1 L of phosphate-buffered saline to remove blood, followed by 4 L of ½ strength Karnovsky's Fixative in 0.1 M sodium phosphate buffer at pH: 7.3 (½ K). The sacral spinal cord was resected and the capsule of connective tissue covering the elongated array matrices was removed with the arrays *in situ*. Spinal roots and nerves were identified to determine the exact level of the array. The array was removed, and the tissue blocks were indexed with a small dot of tissue marking ink on their cut rostral surface, then embedded in paraffin. The paraffin-embedded tissue was cut at a thickness of 8 μm and stained with Nissl or with H&E stains.

We performed immunohistochemical processing for the presence of glial fibrillar acidic protein (GFAP) on several serial sections, usually 8-32 μm lateral to the electrode tips. GFAP is a marker for astrocytes and especially reactive astrocytes, which up-regulate this protein, and as such it is considered to be a marker for disseminated injury in

the CNS. We also wished to determine if GFAP is upregulated during electrical stimulation. In sp104, we examined electrodes #1, #4 and #6. In sp105, we examined sections adjacent to the rostral stabilization pin, and sections that included the tip of unpulsed electrode #3 and sections adjacent to unpulsed electrode # 5.

RESULTS

Figure 1a,b shows the matrices of the circular form-fitting arrays on the dorsal surface of the sacral spinal cord of cats sp104 and sp105. After removal from the spinal cord, the electrode arrays were examined by light and scanning electron microscopy (Figures 2a,b). The histologic analysis showed that all electrodes and stabilization pins in both animals were perpendicular to the longitudinal axis of the cord. It was determined that in sp104, the electrodes were positioned within the S_2 region of the cord and within S_3 in sp105. In sp104, the six electrode tips were located within the ventral dorsal horn and in the intermediate cell column, slightly medial to the intended target, the intermediolateral cell column of S_2 (Figure 3). The tips of the rostral and caudal stabilization pins were located more medially, and within the ventral funiculus (Figure 4). In sp105, in which the array was inserted into S_3 (where the diameter of the cord is less than in S_2), the electrode tips were within the dorsal part of the ventral horns, and the stabilization pins penetrated nearly, or completely through the ventral funiculus (Figure 5). Gliotic scars were associated with the tips of both stabilization pins (Figures 6a, b). Neurons close to the electrode tracks and tips appeared normal, and there was no hyperchromicity to the Nissl stain, and no neuronal shrinkage or chromatolysis. Only one identifiable neuron close to a pulsed electrode (#2 in sp105) appeared to be abnormal (Figure 7). In both cats, a total of three other neurons were observed to be undergoing chromatolysis, but all were more than 1000 μm from the tip of an electrode (Figures 8a, b).

Neurons within 200 μm of the tips of all 12 electrodes from both animals were counted in the 8 μm histological sections that passed directly through the sites of the tips of pulsed or unpulsed electrodes, and in two adjacent 8 μm sections (Figure 9a-d). Table I shows that there were slightly fewer neurons close to the pulsed electrodes, but the difference was not statistically significant ($T=0.78$, $p=0.45$).

TABLE I

ANIMAL & ELECTRODE #	PULSED OR UNPULSED	NEURONS 50-200 μm FROM ELECTRODE TIP (from 3 sections)
sp104		
1	PULSED	16
2	PULSED	23
3	UNPULSED	24
4	UNPULSED	24
5	UNPULSED	9
6	UNPULSED	22
sp105		
1	PULSED	9
2	PULSED	6
3	UNPULSED	14
4	PULSED	3
5	UNPULSED	1
6	UNPULSED	8
		Mean, near pulsed: 11.4
		Mean, near unpulsed: 14.2

As noted above, all six electrodes in cat sp105 penetrated into the ventral horn, because of the smaller diameter of the S_3 cord into which this array was implanted. The histologic findings generally were similar to those from sp104, but there was more gliotic scarring. The intraoperative video indicated that this was due to a transient displacement and flattening of the more tenuously anchored S_3 segment, during electrode insertion. Because of the smaller cross-sectional diameter of the S_3 cord, the array's stabilizing pins

penetrated completely through the ventral surface (Figure 5). However, neurons within 200 μm of the stabilizer pins appeared normal (Figure 10). Neurons close to pulsed and unpulsed electrodes appeared to be normal, and none were undergoing chromatolysis. Figure 11 shows several of these effects, including gliosis, neovascularization and spongy changes in the tissue surrounding the pulsed and unpulsed electrode tips and the stabilization pins. However, these changes were common to pulsed and unpulsed electrodes (Figure 11b,d). Vasculitis and hemosiderin pigments were observed within phagocytic cells along the electrode shafts and stabilization pins, especially in sp105. This indicates that the electrodes inflicted some injury to the parenchymal microvasculature in the immediate vicinity of their tracks, which probably is unavoidable during insertion of electrodes into the CNS. Because it is difficult to depict hemosiderin pigments in black and white photomicrographs, this data is not presented here. However, no larger, space-occupying microhemorrhages were seen, and this is very encouraging.

Other histologic findings included variable, but generally rather minimal gliotic scarring adjacent to the compact glia capsules encasing the electrode shafts, neovascularization in the gray matter and spongy changes within the white matter adjacent to the electrode tips and/or stabilization pins (particularly the latter).

Minimal infiltrations of leukocytes, mainly small, round lymphocytes were observed surrounding the electrode tips and/or shafts. However a 200 μm diameter sphere of cells composed of mixed leukocytes (primarily lymphocytes) and glial cells surrounded the tip of pulsed electrode #1 in cat sp105 (Figures 12a-c). No other association between electrode pulsing and the presence of leukocytes was noted in the two cats. In both cats there was a slight deformation of the cord's dorsal surface, which conformed well to the convex undersurface of the array matrix (Figures 3-6a).

Immunocytochemistry. In both animal, GFAP reaction product was most pronounced within astrocytes and their process adjacent to the compact capsules surrounding the electrodes and stabilization pins (Figures 13a, b). GFAP reaction product was also observed within astrocytic end foot processes embracing small blood vessels, and also surrounding the central canal and associated with the leptomeninges. These

represent normal expressions of GFAP and were not associated with the electrode tracks. No differences in GFAP reactivity were observed between pulsed or unpulsed electrodes in any of the sections evaluated. The increased GFAP reactivity associated with the electrode tracks was confined to the immediate vicinity of the tracks, and this is evidence that the insertion of the electrodes, and their sub-chronic residence in the tissue, was generally well tolerated and did not seriously traumatize the surrounding tissue.

DISCUSSION

The data presented here testifies to the merits of the new bilateral form-fitting electrode array. Firstly, the histologic profiles made by the electrodes and stabilization pins indicate that the spinal cord did not rotate during insertion of the electrodes. The saddle-shaped undersurface of the array matrix also appears to be stable on the cord's dorsal surface. This is in contrast to the previous arrays designs, in which the electrode tracks often were angled obliquely into the cord, and in which there was evidence of slashing of the tissue. Both phenomena are indicative of rotation of the cord during electrode insertion, and/or subsequent mechanical instability of the implanted array. Moreover, while we did observe evidence that the electrodes in cat sp105 initially had penetrated ventral to their final depth (probably due to a transient dorsal-ventral compression and flattening of the S_3 cord during electrode insertion), the damage near the active electrodes was quite minimal. However, we shall not attempt additional insertions into S_3. There was more injury associated with the long stabilizer pins, especially in cat sp105. In the next two animals, we will determine if the pins can be eliminated, and still leave the array with adequate mechanical stability.

We were quite surprised (and pleased) to see GFAP reaction product, since these cats were perfused with ½K fixative containing a high (2.5%) concentration of glutaraldehyde. It is standard procedure in immunohistochemical studies to greatly reduce the concentration of glutaraldehyde, in order to preserve tissue antigenic epitopes. It appears that GFAP is more stable than other antigens, including the CD antigenic markers for leukocytes (Lossinsky et al., 1999; Neuroscience abstract). Our data are consistent with the literature (Duchen, 1992) suggesting the value of this protein as a marker for

astrocytes and especially, for reactive astrocytes. In most of our histologic sections incubated for GFAP, there was a dark granular precipitate that may have masked some details of neuronal morphology. In the future, we will employ the standard peroxidase-diaminobenzidine reaction product which gives a less dense brown precipitate, and this should allow more histologic detail to be visualized. We can then determine if there are changes in GFAP reactivity, as well as changes in other neuron- and glial-specific proteins associated with the electrical stimulation.

Literature Cited

Duchen LW. General pathology of neurons and neuroglia. In: Greenfield's Neuropathology. Eds. Adams, JH, Duchen LW, Fifth Edition, Oxford University Press, New York, 1992, pp. 1-68.

Lossinsky AS, McCreery DB, Bullara LA, Yuen TGH, Agnew WF. Immunohistochemical studies of neuronal, glial, endothelial cell and leukocyte proteins in the feline CNS. Soc for Neurosci [Abstr] 25:208, 1999.

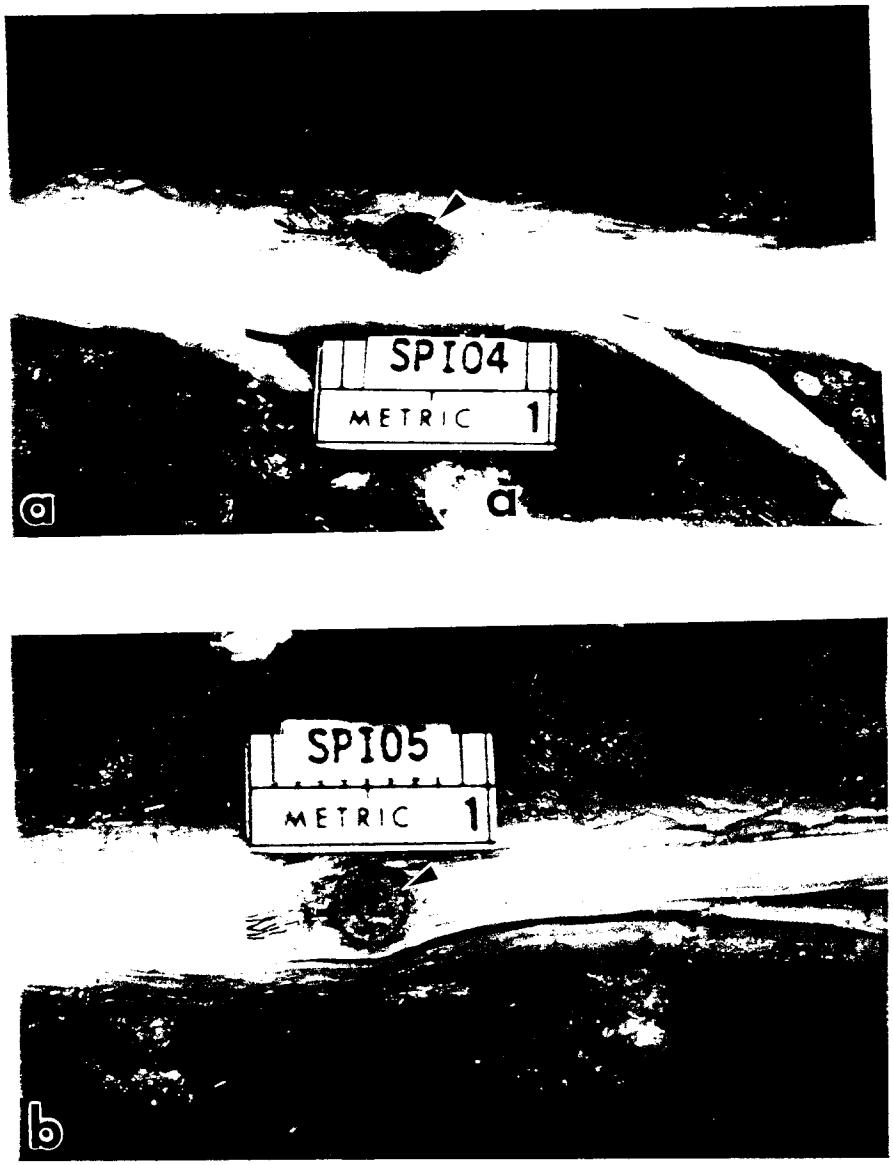

Figure 1a, b. The dorsal surfaces of the lumbosacral region of the cat spinal cord after vascular perfusion fixation. Note the arrays of 6 microelectrodes (arrowheads) in sp104 (a) and sp105 (b). The small gradations of the metric rules represent 1 mm.

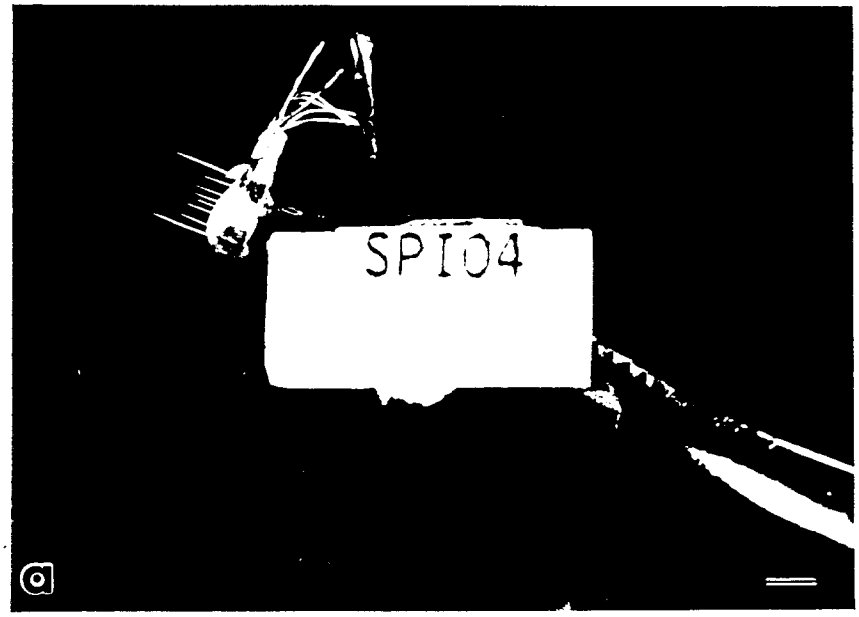

Figure 2a. A slightly magnified view of a six electrode array from cat sp104, immediately after its removal from the spinal cord. To facilitate its removal from the spinal cord, the array was glued with cyanoacrylate to a knot at the end of a suture. Note the two long stabilization pins and the shorter microelectrodes. Bar = 3 mm.

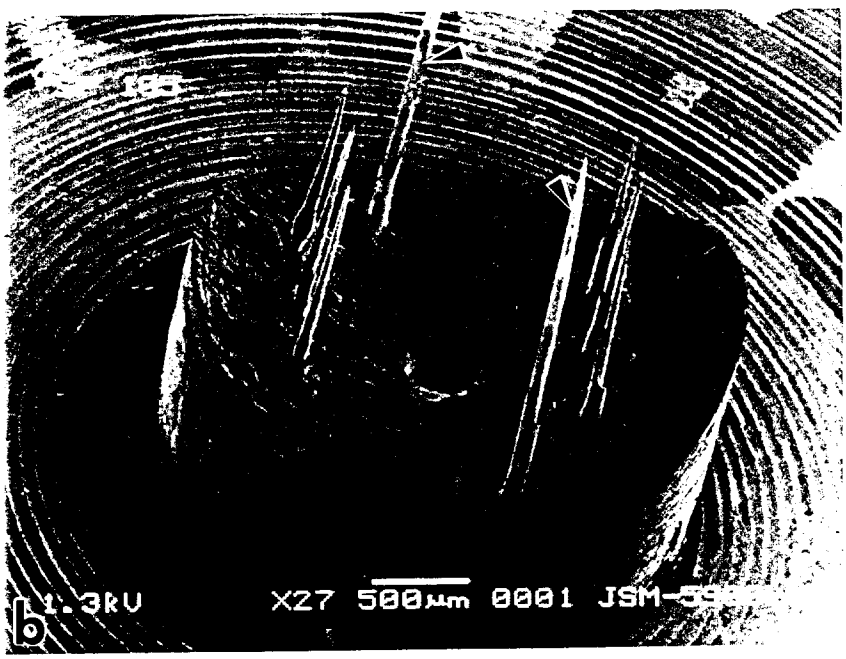

Figure 2b. Scanning electron micrograph of the undersurface of the array from sp105. Note the long stabilization pins (arrowheads) shown in Figure 2 and the two rows of shorter electrodes. White bar = 500 µm.

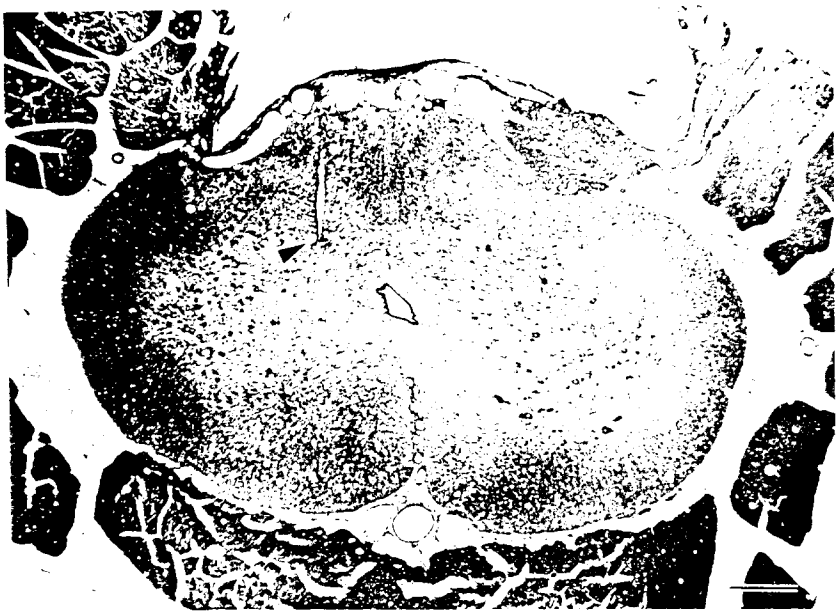

Figure 3. The track of pulsed electrode #1 from sp104. The electrode tip (arrowhead) is shown medial to the intermediolateral cell column. Note the slight compression of the dorsal surface of the cord produced by the undersurface of the array.
Nissl stain. Bar = 500 µm.

Figure 4. Sp104. Caudal stabilization pin. The tip of the stabilization pin (arrowhead) was within the ventral funiculus. Nissl stain. Bar = 500 µm.

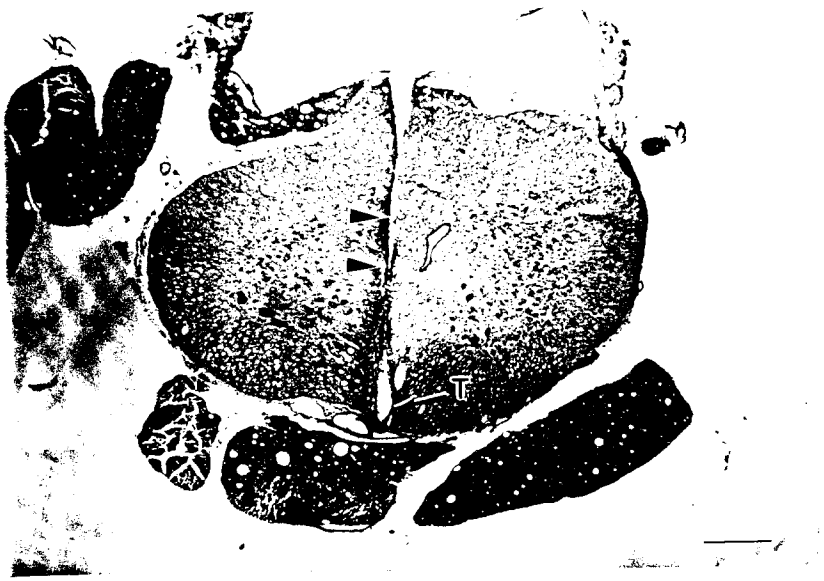

Figure 5. Sp105. The track made by the rostral stabilization pin (arrowheads) is shown, the tip (T→) of which has penetrated through the ventral funiculus. Nissl stain. Bar = 500 µm.

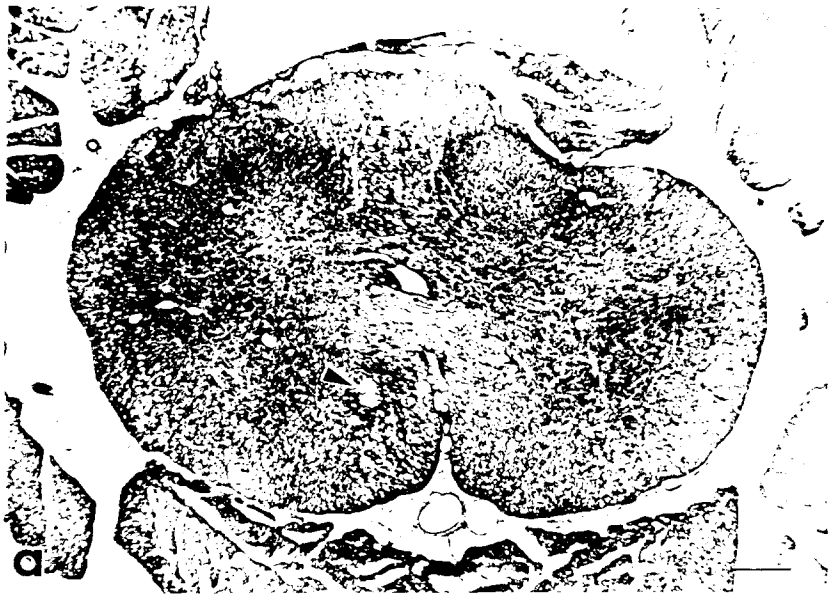

Figure 6a. Sp104. A gliotic scar produced by one of the stabilization pins within the ventral funiculus (arrowhead). Nissl stain. Bar = 500 µm.

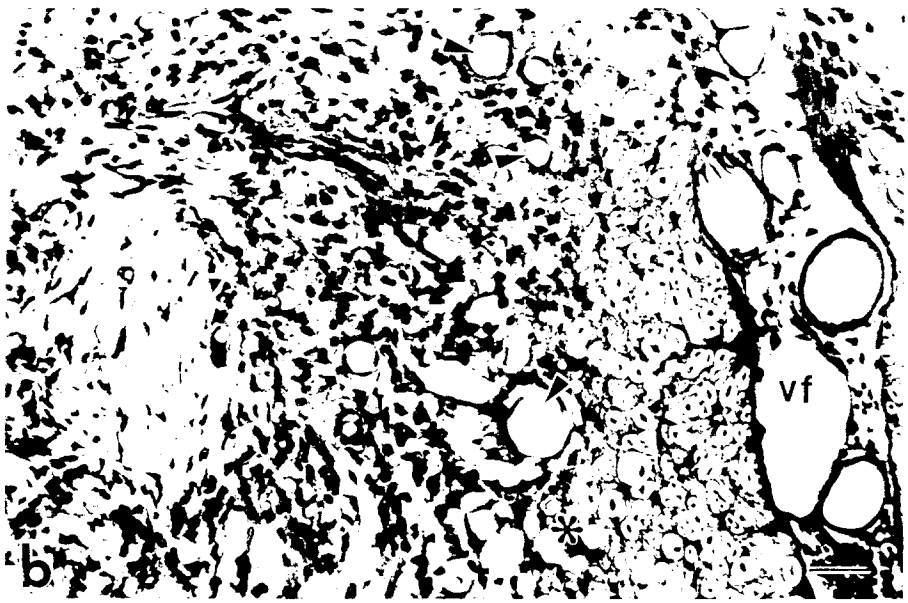

Figure 6b. Higher magnification of the gliotic scar shown in Figure 6a. Note the neovascularization (arrowheads) and spongy changes within the white matter (*) adjacent to the ventral fissure (vf). Nissl stain. Bar = 100 µm.

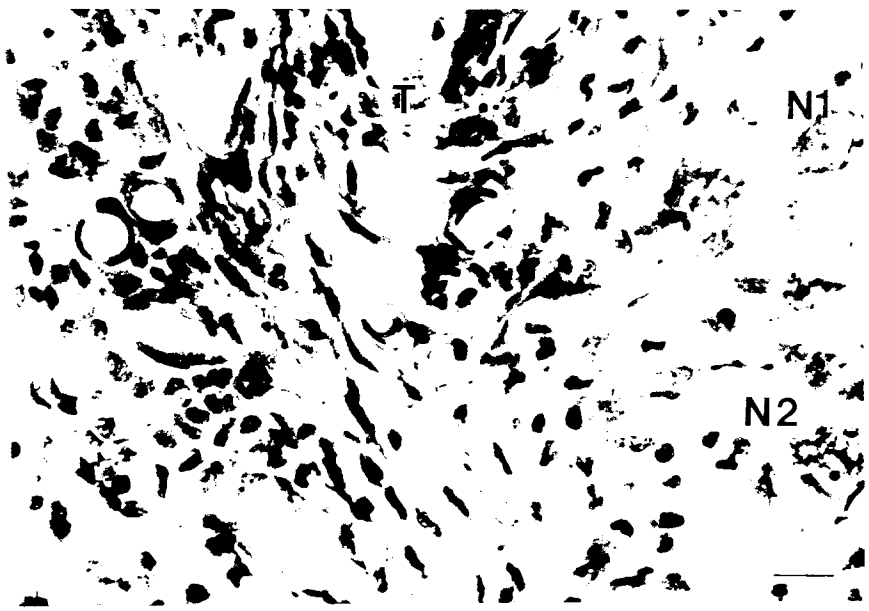

Figure 7. Sp105. The site of the tip (T) of pulsed electrode #2 and two neurons within 150 µm of the tip. One neuron (N1) appears normal while another (N2) shows clumping of the Nissl substance . Nissl stain. Bar = 25 µm.

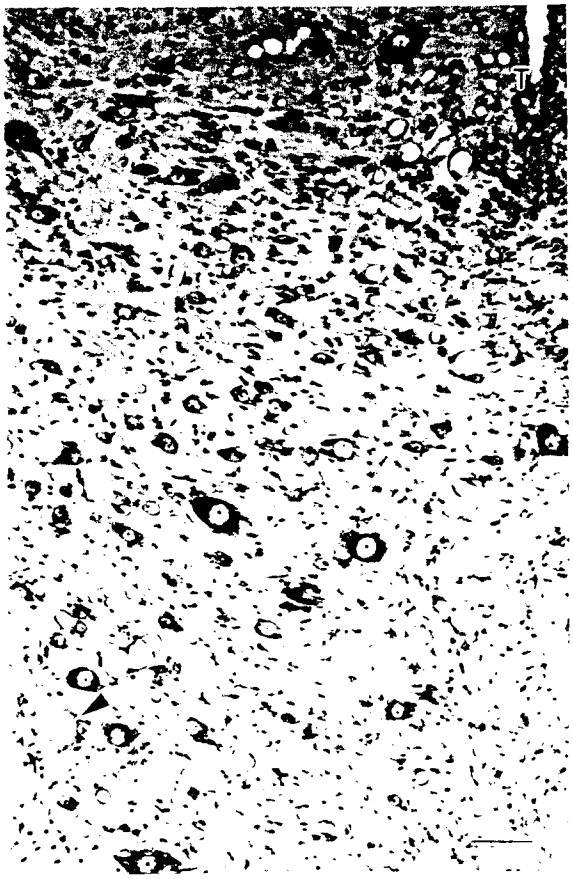

Figure 8a. Sp104. Pulsed electrode #2. A single chromatolytic neuron (arrowhead) is shown approximately 1000 µm from the electrode tip (T). Nissl stain. Bar = 50 µm.

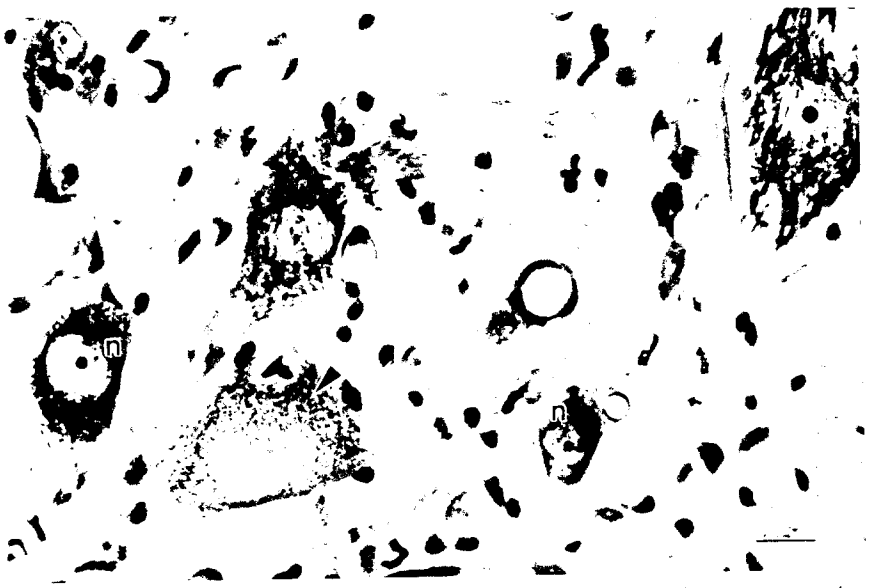

Figure 8b. Higher magnification of the region of the chromatolytic neuron shown in Figure 8a. Note the sparse Nissl substance in the chromatolytic cell (arrowhead) and the nearby normal-appearing neurons (n). H&E stain. Bar = 25 µm.

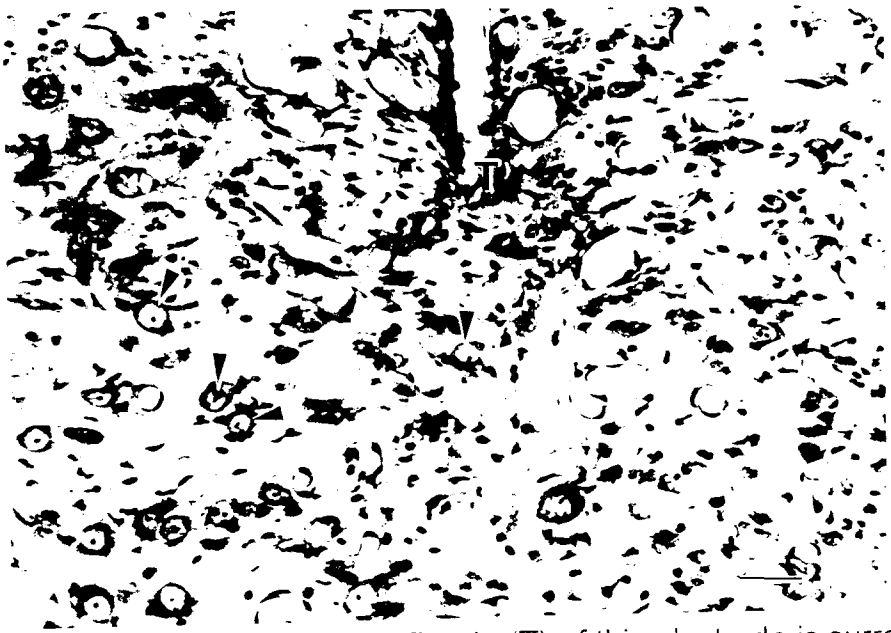

Figure 9a. Sp104, pulsed electrode #1. The tip (T) of this electrode is surrounded by four small, normal-appearing neurons (arrowheads). Nissl stain. Bar = 50 µm.

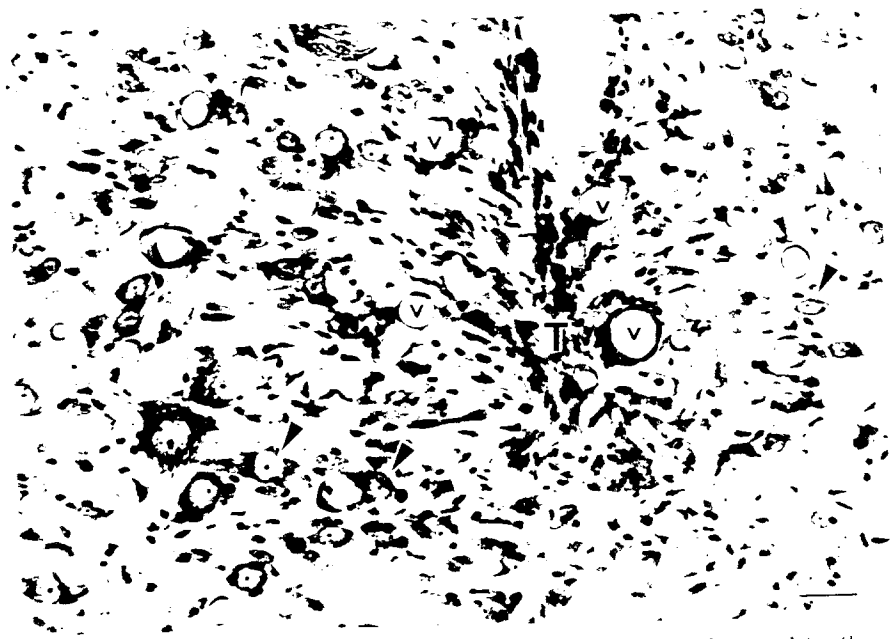

Figure 9b. Sp104, pulsed electrode #1. This section is 16 µm lateral to the site of the electrode tip shown in 9a. Its approximate location behind the section is indicated (T). Several normal-appearing neurons (arrowheads) are shown. Neovascularization (v), and minimal gliosis (reactive astrocytes) are also shown. Nissl stain. Bar = 50 µm.

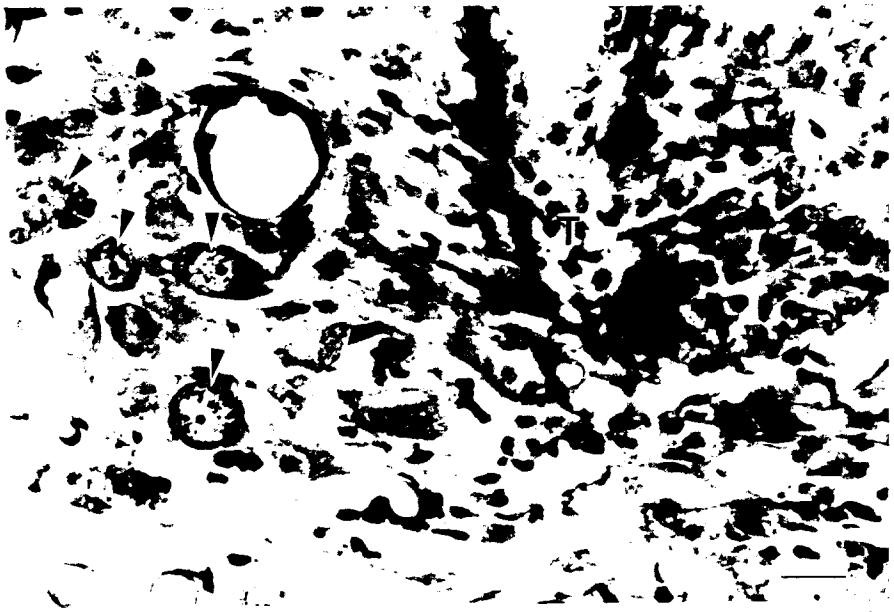

Figure 9c. Sp104. pulsed electrode #2. The site of the electrode tip (T), and a cluster of four small, normal-appearing neurons (arrowheads) are shown. Nissl stain. Bar = 25 µm.

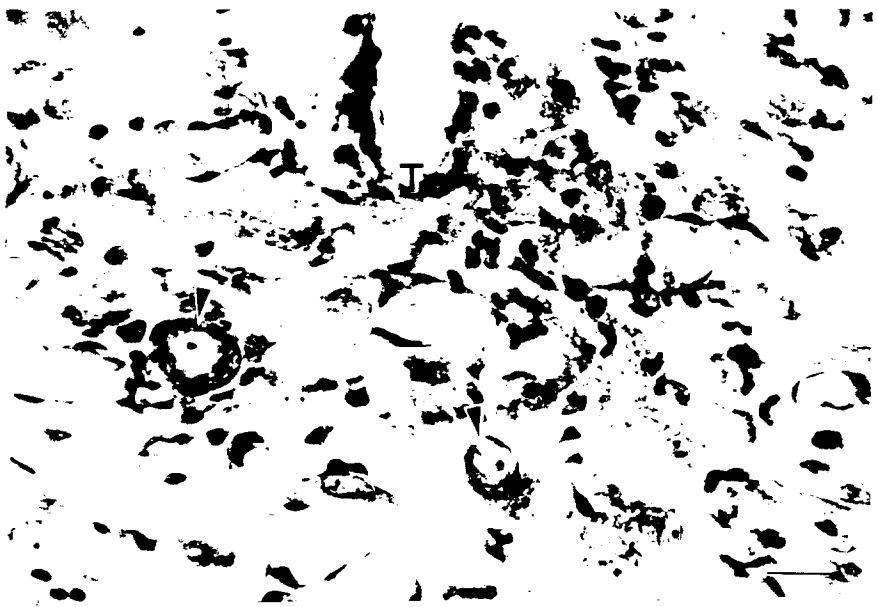

Figure 9d. Sp104. Unpulsed electrode #3. Two normal-appearing neurons (arrowheads) are within 150 µm of the site of the electrode tip (T). Nissl stain. Bar = 25 µm.

Figure 10. Sp105. Gliosis adjacent to the rostral stabilization pin (s). Several normal-appearing neurons (n) are within 200 µm of the gliotic scar surrounding the pin. Nissl stain. Bar = 50 µm.

Figure 11a. Sp105. The track of pulsed electrode #4, within the ventral horn (arrowheads). Nissl stain. Bar = 500 µm.

Figure 11b. Higher magnification of the electrode tip site shown in Figure 11a. Note the gliosis (*), neovascularization (v), spongy changes (s) and the normal-appearing neurons (arrowheads) within 200 µm of the tip site (T). Nissl stain. Bar = 50 µm

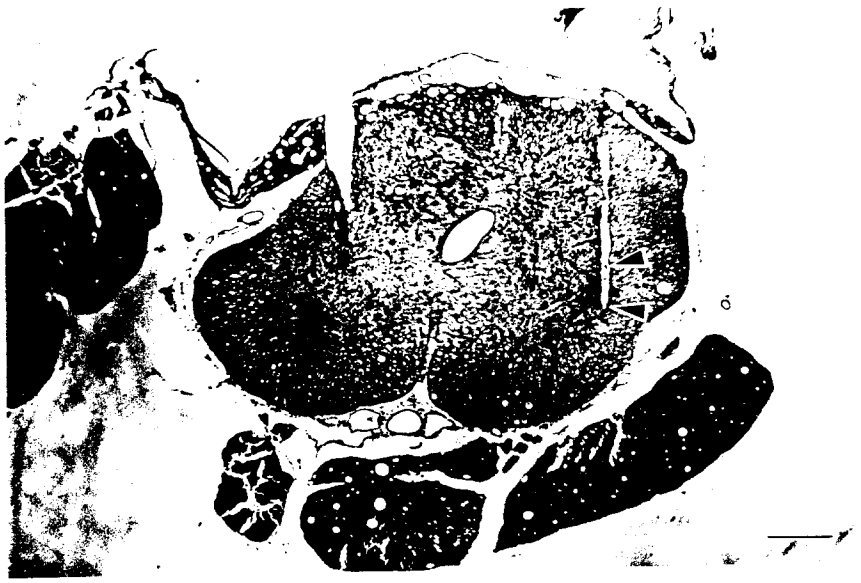

Figure 11c. sp105. The track of unpulsed electrode #5, within the ventral horn (arrowheads). Nissl stain. Bar = 500 µm

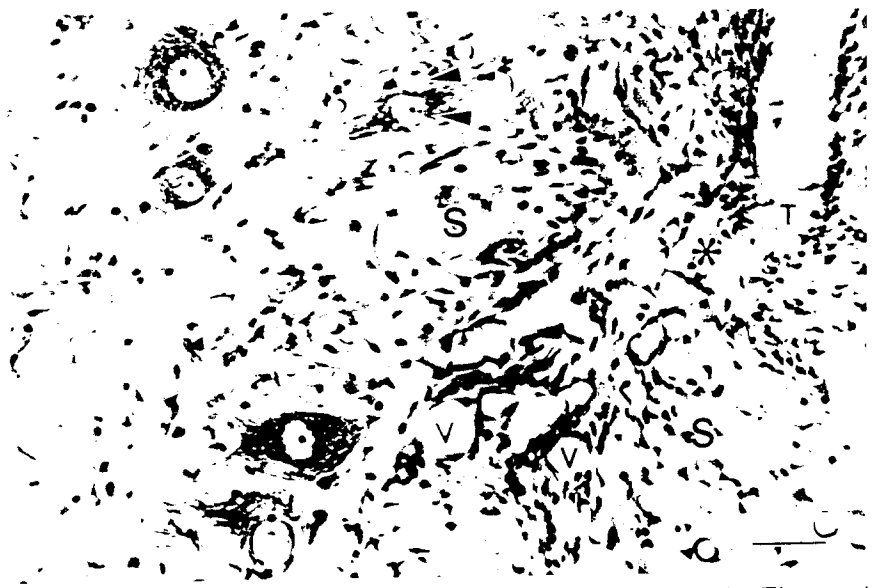

Figure 11d. Higher magnification of the electrode tips site shown in Figure 11c. Note the gliosis (*), neovascularization (v), spongy changes (s) and the normal-appearing neurons (arrowheads) within 200 µm of the tip site (T). Nissl stain. Bar = 50 µm

Figure 12a. Sp105. The track and tip site (arrowhead) of pulsed electrode #1. Nissl stain. Bar = 500 µm.

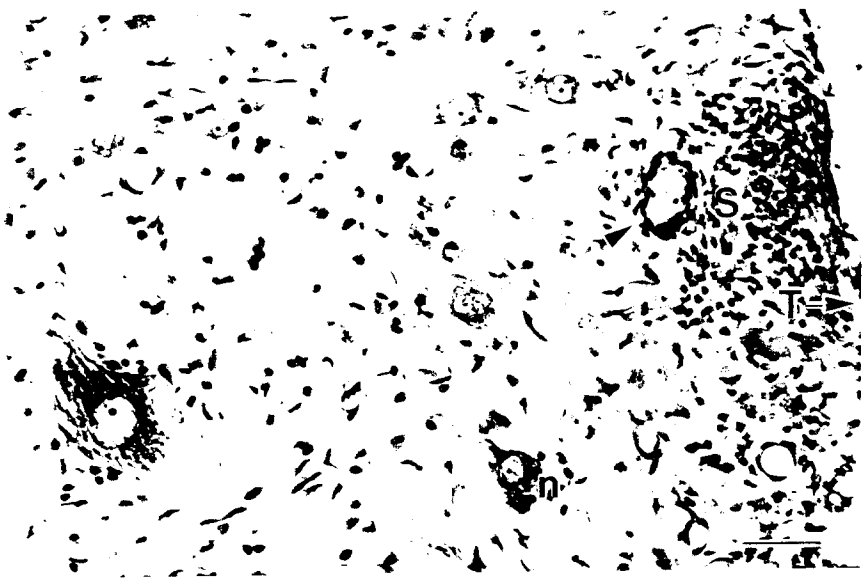

Figure 12b. Higher magnification of the region of the tip (T→) of the electrode shown in 12a. Note the darkly-stained, scattered small round cells (presumably lymphocytes) within the glial cell sheath (s). A small perivascular cuff of lymphocytes is seen surrounding one blood vessel (arrowhead). One normal-appearing neuron (n) is within 150 µm of the electrode tip. Nissl stain. Bar = 50 µm.

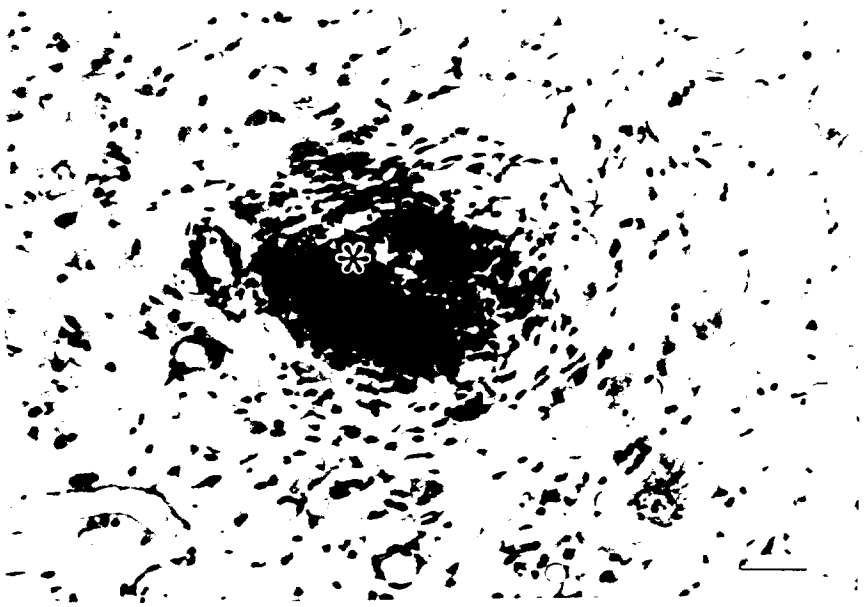

Figure 12c. A section 16 µm from the section shown in Figure 12a, b. Note the dense accumulation of small, round cells (presumable lymphocytes) within the small glial scar (*) surrounding the site of the electrode tip. H&E stain. Bar = 50 µm.

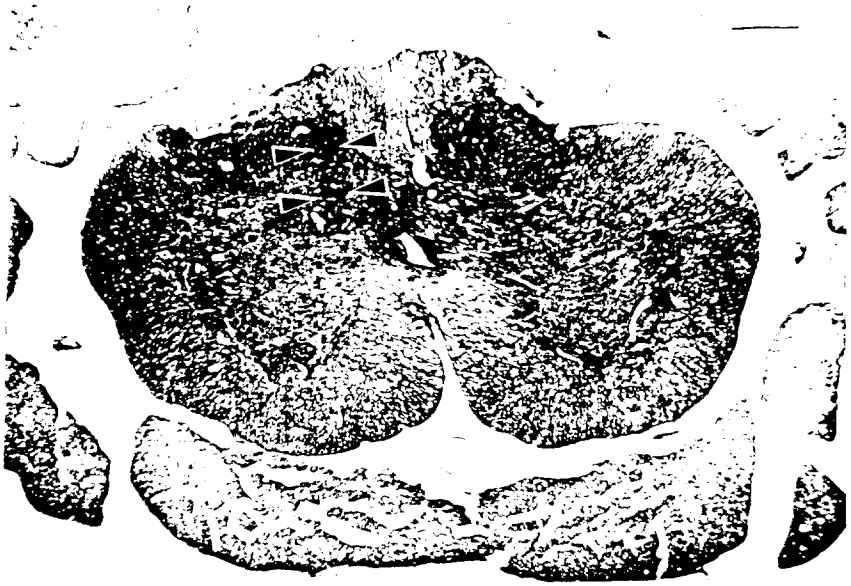

Figure 13a. Sp104. GFAP immunohistochemical reaction and hematoxylin stain. This micrograph shows a tissue section adjacent to the tip of pulsed electrode #2. The arrowheads delimit the region darkened by the GFAP reaction. Bar = 500 µm.

Figure 13b. Higher magnification of the region adjacent to the electrode track shown in Figure 13a. Note the cells composing the electrode sheath (s) and several larger GFAP-positive reactive astrocytes adjacent to the sheath (arrowheads). GFAP immunohistochemical reaction, hematoxylin stain. Bar = 25 µm.